

Structures of the Reduced and Mercury-Bound Forms of MerP, the Periplasmic Protein from the Bacterial Mercury Detoxification System^{†,‡}

Ruth A. Steele and Stanley J. Opella*

Department of Chemistry, University of Pennsylvania, Philadelphia, Pennsylvania 19104

Received December 27, 1996; Revised Manuscript Received March 7, 1997[⊗]

ABSTRACT: Bacteria carrying plasmids with the *mer* operon, which encodes the proteins responsible for the bacterial mercury detoxification system, have the ability to transport Hg(II) across the cell membrane into the cytoplasm where it is reduced to Hg(0). This is significant because metallic mercury is relatively nontoxic and volatile and thus can be passively eliminated. The structures of the reduced and mercury-bound forms of merP, the periplasmic protein, which binds Hg(II) and transfers it to the membrane transport protein merT, have been determined in aqueous solution by multidimensional NMR spectroscopy. The 72-residue merP protein has a $\beta\alpha\beta\beta\alpha\beta$ fold with the two α helices overlaying a four-strand antiparallel β sheet. Structural differences between the reduced and mercury-bound forms of merP are localized to the metal binding loop containing the consensus sequence GMTCCXXC. The structure of the mercury-bound form of merP shows that Hg(II) is bicoordinate with the Cys side chain ligands, and this is confirmed by the chemical shift frequency of the ¹⁹⁹Hg resonance.

There are enormous amounts of heavy metals in the environment. Organometallic compounds resulting from various types of industrial and military waste are of particular concern. These metals and their compounds are nearly universally toxic to biological organisms including humans because of their nonselective chemistry; for example, since Hg(II) reacts with essentially all exposed sulfhydryl groups on proteins, it interferes with a wide range of biological functions (Walsh et al., 1988). Therefore, it is surprising to find that some bacteria thrive in the presence of high concentrations of heavy metal toxins. This is possible only because these bacteria possess efficient mechanisms for the detoxification of heavy metals (Summers et al., 1986). A plausible explanation for the presence of these mechanisms is that since the earth's prebiotic environment was undoubtedly heavily polluted with heavy metals from geochemical processes, the most primitive organisms had to evolve ways for dealing with heavy metals so that Cys, His, and other amino acids with side chains capable of binding to metals could be utilized in their proteins. Regardless of the initial sources, genes associated with bacterial resistance to a wide variety of toxic metals have been described (Silver, 1992; Silver & Waldeshaug, 1995).

The most thoroughly investigated bacterial mercury detoxification system is remarkable. It functions by transporting toxic Hg(II) into the cell where it is converted to relatively nontoxic metallic Hg(0) which is volatile and can be passively eliminated (Brown, 1985; Foster, 1987; Summers, 1986). The sequences of the proteins responsible for mercury detoxification are encoded in the *mer* operon on a plasmid

that typically also has operons that confer antibiotic resistance (Foster, 1987). The *mer* operon consists of several structural genes whose expression is regulated by the merR repressor protein (O'Halloran et al., 1993). The merP (periplasm) protein binds mercury in the periplasm and transfers it to the merT (transport) protein responsible for transporting mercury through the membrane into the cytoplasm (Brown, 1985; Lund & Brown, 1987). Other components of the system include the enzymes mercuric reductase, which reduces Hg(II) to Hg(0) in the cytoplasm (Schiering et al., 1991), and organomercury lyase (Foster, 1987), which removes organic ligands from Hg(II).

In addition to their direct biological toxicity through damage to proteins, heavy metals are involved in several human diseases where transport functions are perturbed. For example, both Menkes and Wilson diseases result from improper copper metabolism, and the genes responsible for these diseases have been shown to correspond to P-type ATPases containing multiple repeats of a metal binding domain with sequences highly homologous to that of merP (Lutsenko & Kaplan, 1995). Indeed, mutations in the merP-like domains of these proteins are associated with human diseases (Chelly et al., 1993; Mercer et al., 1993). Further, a possible connection has been found between the mercury in dental amalgam fillings and antibiotic resistance in oral and intestinal bacteria because those bacteria with plasmids containing both *mer* and antibiotic resistance operons are

[†] This research was supported by Grants R823576 from the Environmental Protection Agency, AI20770 from the National Institutes of Health, and DAAL 03-92-6-0713 from the U.S. Army Research Office.

[‡] Coordinates have been deposited in the Brookhaven Protein Data Bank (filenames 1afi and 1afj).

* Corresponding author. Phone: (215) 898-6459. FAX: (215) 573-2123. E-mail: opella@chestnut.chem.upenn.edu.

[⊗] Abstract published in *Advance ACS Abstracts*, May 1, 1997.

¹ Abbreviations: CBCACONH, C^β carbon to C^α to carbonyl carbon to amide proton correlation; DTT, dithiothreitol; EDTA, ethylenediaminetetraacetic acid; FHSQC, fast heteronuclear single-quantum coherence; HMQC, heteronuclear multiple-quantum coherence; HNHA, amide proton to nitrogen to C^αH proton correlation; HNCA, amide proton to nitrogen to C^α carbon correlation; HSQC, heteronuclear single-quantum coherence; IPTG, isopropyl thiogalactoside; MBP, maltose binding protein; NMR, nuclear magnetic resonance; NOE, nuclear Overhauser effect; NOESY, nuclear Overhauser enhancement spectroscopy; PCR, polymerase chain reaction; rmsd, root mean square deviation; TOCSY, total correlation spectroscopy; TPPI, time-proportional phase incrementation; SA, simulated annealing.

selected by the release of mercury from the dental fillings (Lorscheider et al., 1995). Interest in these proteins also results from their potential use in bioremediation, including their expression in plants for removal of heavy metals in soils (Rugh et al., 1996).

We are using NMR¹ spectroscopy to determine the structures of the proteins responsible for the initial recognition, binding, and transport of mercury through the cell membrane in the bacterial mercury detoxification system. MerP and merT, in particular, are attractive candidates for structural studies because they are small, with 72 residues (77 as expressed) in the case of merP and 116 residues (122 as expressed) for merT. MerP is soluble in aqueous solution and gives well-resolved two- and three-dimensional NMR spectra, enabling its structure to be determined by multidimensional solution NMR spectroscopy as described in this paper. MerT, which is an intrinsic membrane protein, requires a combination of solution NMR and solid-state NMR methods for its structure determination in micelle and bilayer environments (Opella, 1994). The studies of merP and merT, in combination with the ongoing structural studies on the merR repressor (Ansari et al., 1992) and mercuric reductase (Schiering et al., 1991) and organomercury lyase enzymes (Ralston & O'Halloran, 1990; Helmann et al., 1990), should provide considerable insight into the chemistry and structural biology of the bacterial detoxification system. The secondary structure and overall fold of oxidized merP in solution determined by ¹H NMR spectroscopy has been previously reported (Eriksson & Sahlman, 1993). This paper describes the three-dimensional structures of the reduced and mercury-bound forms of merP in solution determined by heteronuclear multidimensional NMR spectroscopy.

MATERIALS AND METHODS

Materials. Oligonucleotide primers were synthesized by the University of Pennsylvania Cancer Center Nucleic Acid Facility. The plasmid pHK1 containing the merP gene was provided by Nancy Hamlett, assisted by Matt Harris and Dave Karlton (Swarthmore College). Competent DH5 α *Escherichia coli* cells were purchased from GibcoBRL (Gaithersburg, MD), and cells of strain BL21/BL21(DE3) were purchased from Novagen (Madison, WI). The plasmid vector pMAL-c2, protease factor Xa, amylose affinity resin, and T4 DNA ligase were purchased from New England Biolabs (Beverly, MA). Restriction enzymes *Eco*RI and *Hind*III were purchased from GibcoBRL (Gaithersburg, MD). A Sequenase version 2.0 DNA sequencing kit was purchased from United States Biochemical (Cleveland, OH). The PCR core kit was from Boehringer Mannheim Biochemicals (Indianapolis, IN). The protease inhibitors leupeptin and pepstatin A were from Boehringer Mannheim Biochemicals (Indianapolis, IN). Gel filtration medium Sephacryl S-100 was obtained from Pharmacia LKB (Piscataway, NJ). Isotopic labeling utilized (¹⁵NH₄)₂SO₄ (Cambridge Isotope Laboratories, Andover, MA, or Isotec, Miamisburg, OH), ¹³C glucose (Cambridge Isotope Laboratories, Andover, MA), or ¹³C/¹⁵N algal media from Isogenetics (Chicago, IL). ¹⁹⁹HgO (85.5%) was purchased from Isotec (Miamisburg, OH). Rapid Pure Minipreps, RPM kits from Bio 101, Inc. (La Jolla, CA), were used for small-scale plasmid preparations.

Construction of Expression Vector pSSS. The merP gene was amplified by PCR from pHK1 by using forward and

reverse primers. The plasmid pHK1 is a construct containing the merP gene from the transposon Tn21 (on plasmid R100) which originated from a *Shigella flexneri* strain of bacteria found in Japan in 1959 (Misra et al., 1984). The sequence for the forward primer was 5'ATATTGAATTCATGGC-TACCCAGACGGTCACGCTA^{3'}, and that for the reverse primer was 5'TAATTAAGCTTAATCACTGCTTGACGCTG-GACGG^{3'}, where the underlined sequence is from the merP gene and the sequence in bold is for the designed restriction sites *Eco*RI and *Hind*III, respectively. In lightface type are the flanking bases needed for the restriction enzymes to work effectively. The primers were designed to introduce an *Eco*RI site at the start of the merP gene and a *Hind*III site at the end. The PCR product was digested with *Eco*RI and *Hind*III and ligated into similarly digested pMAL-c2. The recombinant plasmid (pSSS) was transformed into competent DH5 α *E. coli* cells. Successful transformants were screened by restriction digestion using a unique *Nhe*I site within the merP gene. The DNA sequence was confirmed by the dideoxy sequencing method (Sanger et al., 1977). Supercoiled plasmid was isolated from the DH5 α strain and retransformed into BL21 *E. coli* cells which grow well in the minimal media used for isotopic labeling.

Expression of MerP. Uniformly ¹⁵N-labeled and ¹³C/¹⁵N-labeled merP were obtained by expression in minimal M9 media (11 g/L Na₂HPO₄·7H₂O, 3 g/L KH₂PO₄, 0.5 g/L sodium citrate, ~10 mg of thiamin, 1 mL of 1 M MgSO₄/MgCl₂, 0.1 mL of CaCl₂) containing 1 g/L (¹⁵NH₄)₂SO₄ and 2 g/L [¹³C]glucose (10 g/L unlabeled glucose) or by using ¹³C/¹⁵N-labeled algal media. A 1 mL culture in rich LB media was used to inoculate 25 mL of minimal media which was grown overnight. This was then used to inoculate 1 L of minimal media. The bacteria were grown to an OD₅₅₀ of about 0.5 before induction with IPTG (final concentration 0.5 mM). Incubation was continued for 2–3 h before being harvested by centrifugation. All cultures were maintained at 37 °C and contained 100 μ g/mL ampicillin. Cells were immediately frozen and kept at –80 °C until further use.

Purification of MerP. Protein purification was monitored at each stage by Tris–tricine gel electrophoresis (von Schägger & Jagow, 1987). Where possible, all procedures were carried out at 4 °C. Cells from 1 L of growth media were resuspended in 20 mL of 20 mM sodium phosphate (pH 7.5) buffer containing 10 μ g/mL lysozyme, 0.01% sodium azide, 50 mM dithiothreitol (DTT), and the protease inhibitors pepstatin A and leupeptin (1 μ g/mL). For the preparation of merP in the reduced form, the buffer also contained 1 mM EDTA. The cell suspension was passed through a French press twice at 12 000 psi, and the resulting lysate was cleared by centrifugation at 50 000g for 45 min at 4 °C. The supernatant was diluted to 100 mL with additional buffer and then passed over an amylose resin affinity column which bound the MBP-merP fusion protein. The column was washed with 3 volumes of 20 mM sodium phosphate (pH 7.5) to remove the unbound proteins. The fusion protein was eluted with sodium phosphate containing 10 mM maltose. All fractions containing fusion protein were combined and concentrated to \geq 1 mg/mL (typically 50 mL/L of original growth media) using a YM30 membrane in an Amicon stirred cell. The fusion protein was cleaved with factor Xa at a concentration of 10 μ g/mL for 1–2 days. After complete cleavage, DTT was immediately added to a concentration of 10 mM. The cleavage products were

Table 1: NMR Acquisition Parameters

NMR experiments	nucleus			no. of points			spectral width (ppm)			final matrix size			scans
	F_1	F_2	F_3	F_1	F_2	F_3	F_1	F_2	F_3	F_1	F_2	F_3	
Reduced MerP													
HMQC/FHSQC	^{15}N	^1H		128–256	2048		35	12		256–512	896 ^a		
^{15}N -edited TOCSY	^1H	^{15}N	^1H	120		2048	12	35	12	256	128	896 ^a	24
^{15}N -edited NOESY	^1H	^{15}N	^1H	220		2048	12.5	35	12.5	512	128	896 ^a	16
NOESY	^1H	^1H		512		2048	12	12		1024	2048		32
TOCSY	^1H	^1H		512		2048	12	12		1024	2048		32
HNHA	^{15}N	^1H	^1H	72	80	2048	35	12	12	128	128	442 ^a	32
HNCA	^{15}N	^{13}C	^1H	44	60	1024	35	35	12	128	128	442 ^a	16
HNCOCA	^{15}N	^{13}C	^1H	40	64	2048	35	35	12	128	128	448 ^a	16
CBCACONH	^{13}C	^{15}N	^1H	64	44	1024	56	36	12	256	128	448 ^a	16
T_1 HSQC	^{15}N	^1H		190	1024		35	12		512	1024		16
T_2 HSQC	^{15}N	^1H		150	1024		35	12		512	1024		32
HXNOE	^{15}N	^1H		128	1024		35	12		256	1024		32
Mercury-Bound MerP													
HMQC/FHSQC	^{15}N	^1H		128–256	2048		35	12		256–512	896		var
^{15}N -edited TOCSY	^1H	^{15}N	^1H	120		2048	12	35	12	256	128	896 ^a	24
^{15}N -edited NOESY	^1H	^{15}N	^1H	220		2048	12.5	35	12.5	512	128	896 ^a	16
NOESY	^1H	^1H		896		2048	12	12		1024	2048		48
TOCSY	^1H	^1H		512		2048	12	12		1024	2048		16
HNHA	^{15}N	^1H	^1H	60	120	2048	35	12	12	128	128	442 ^a	24
T_1 HSQC	^{15}N	^1H		190	1024		35	12		512	1024		16
T_2 HSQC	^{15}N	^1H		148	1024		35	12		512	1024		96
HXNOE	^{15}N	^1H		128	1024		35	12		256	1024		32

^a Spectra were strip transformed in this dimension to include only the amide region (low field) part of the spectrum.

concentrated to 2 mL using a YM3 membrane and then applied to a Sephacryl S-100HR column (90 × 2.5 cm, Pharmacia, Piscataway, NJ) equilibrated with 20 mM sodium phosphate (pH 7.5) buffer, 0.01% sodium azide, 10 mM DTT, 1 mM EDTA (reduced samples only), and the protease inhibitors pepstatin A and leupeptin (1 μg/mL). As judged by silver-stained gel electrophoresis, the protein is very pure (>95%). The solution containing merP was concentrated to 1–3 mM and dialyzed against the buffer used in the NMR samples.

Sample Preparation. Samples for NMR studies contained 1–3 mM protein in 20 mM phosphate buffer (pH 6.5) in 90% H₂O/10% D₂O or 100% D₂O. Samples with the mercury-bound form of merP were prepared by carefully titrating Hg²⁺ (typically HgCl₂) into a previously prepared reduced merP sample until the NMR spectra stopped changing (approximately 1:1.5 [protein]:[Hg²⁺]). For ¹⁹⁹Hg NMR samples, ¹⁹⁹HgO was dissolved in concentrated phosphoric acid and then diluted to make a stock solution. After addition of ¹⁹⁹Hg²⁺ the sample pH was readjusted to 6.5.

NMR Spectroscopy. All NMR spectra were recorded at 300 K on Brüker DMX500, DMX600, and DMX750 NMR spectrometers. NMR spectra were processed using XWIN-NMR (Brüker) or Felix (Biosym) and analyzed using NMRCOMPASS (Molecular Simulations). All of the pulse sequences incorporated WATERGATE (Piotto et al., 1992), except where noted, for suppression of the water resonance. ¹⁵N decoupling was performed using the GARP sequence (Shaka et al., 1985). Mild exponential line broadening in the acquisition (¹H) dimension (1–5 Hz) and a shifted (60–90°) squared sine bell in the indirect dimensions (¹⁵N, ¹³C) were applied to the free induction decays except where indicated.

Two-dimensional ¹H–¹⁵N heteronuclear FHSQC (Mori et al., 1995) and HMQC (Bax et al., 1983) spectra were used to characterize the protein samples and as the starting point for the NMR studies. ¹⁵N resolved three-dimensional

NOESY/HMQC experiments (Marion et al., 1989) were performed using mix times of 100, 125, and 250 ms. The ¹⁵N resolved three-dimensional TOCSY/HMQC spectra (Marion et al., 1989) were obtained with a mix time of 80 ms (MLEV) (Levitt, 1982) for both reduced and mercury-bound forms of merP. Two-dimensional ¹H–¹H NOESY and TOCSY spectra were obtained from samples of reduced and mercury-bound merP in D₂O solution. The signal from residual HDO in the samples was suppressed with weak continuous irradiation of the water resonance during the recycle delay. NOESY spectra were acquired with mix times of 50 and 125 ms. TOCSY spectra were acquired with a mix time of 80 ms. ³J_{HN,Hα} coupling constants were measured with three-dimensional HNHA experiments (Vuisster & Bax, 1993). Water suppression was achieved with weak irradiation at the water resonance during the recycle delay. Backbone resonance assignments were made using the HNCA (Kay et al., 1990), HNCOCA (Bax & Ikura, 1991), and CBCA (Gresiek & Bax, 1992) three-dimensional triple-resonance experiments. WEX filter (Mori et al., 1994) experiments were performed using a two-dimensional HMQC version of the published pulse sequence with the WEX filter placed before the start of the HMQC pulse sequence. The second ¹H 90° pulse of the WEX filter was substituted for the first 90° pulse of the HMQC sequence. Other parameters are described in Table 1. The mix times varied between 25 and 250 ms.

The one-dimensional ¹⁹⁹Hg NMR spectrum was acquired using a direct-detect 10 mm broad-band probe at 89.5 MHz on the DMX500 spectrometer. The sample volume was 1 mL, and the protein concentration was approximately 3 mM with an approximately 20% excess of 85.3%-enriched ¹⁹⁹Hg²⁺ in the solution. The spectrum was acquired with 450 000 scans in about 20 h with a sweep width of 200 kHz, a 20° pulse, and 150 ms recycle delay. It was processed with 1000 Hz of line broadening. The first few points of the FID were replaced by linear prediction to remove a

baseline roll in the spectrum. The spectrum was referenced with respect to neat dimethylmercury at 0 ppm.

T_1 and T_2 relaxation times were measured on the DMX600 spectrometer using two-dimensional ^1H -detected ^{15}N heteronuclear experiments (Kay et al., 1992) with the addition of gradient water suppression and gradient filters for artifact suppression. T_1 relaxation times were measured from ten two-dimensional data sets with relaxation delays of 10 ms, 50 ms, 100 ms, 200 ms, 300 ms, 500 ms, 600 ms, 800 ms, 1 s, and 1.5 s. T_2 relaxation times for mercury-bound merP were measured from six two-dimensional data sets with relaxation delays of 8, 16, 24, 40, 56, and 80 ms. Values for reduced merP were determined from seven data sets with relaxation delays of 8, 15, 22, 38, 45, 68, and 90 ms taken with $150 (t_1, ^1\text{H}) \times 1024 (t_2, ^1\text{H})$ points and 32 scans per increment. Processing in the $t_2 (^1\text{H})$ dimension was done with Gaussian multiplication for resolution enhancement to maximize the number of residues for which relaxation times could be measured.

Heteronuclear ^1H - ^{15}N NOEs were measured on a DMX600 spectrometer in the absence and presence of ^1H saturation (Kay et al., 1989) which was accomplished with the application of 120° pulses at 20 ms intervals for 5 s before the first ^{15}N pulse. Control experiments had a 5 s recycle delay to replace this ^1H saturation period and ensure both experiments were the same length. To minimize the effects of chemical exchange between water and amide protons on the value of the measured NOE, experiments were performed with gradient water suppression and water flip-back techniques (Grzesiek & Bax, 1993b; Piotto et al., 1992). Experiments for both forms of merP were performed with $128 (t_1, ^1\text{H}) \times 1024 (t_2, ^1\text{H})$ points and 32 scans per increment.

Dynamics. All fitting of the experimental relaxation data was performed using the computer programs of Farrow et al. (1994). T_1 and T_2 values were determined by fitting the measured intensities of the peaks to a two-parameter equation for exponential decay. The steady-state NOE values were determined from the ratio of the intensities of the peaks with and without ^1H saturation. The root mean square of the background noise from each experiment was used as an estimate of the standard deviation of the measured intensities.

A model-free formalism as expressed by eq 1 was used to fit the experimental data (Lipari & Szabo, 1982a,b)

$$J(\omega) = \frac{S^2\tau_m}{(1 + \omega^2\tau_m^2)} + \frac{(1 - S^2)\tau}{(1 + \omega^2\tau^2)} \quad (1)$$

where the order parameter S^2 describes the degree of spatial restricted motion of the ^1H - ^{15}N bond vector and τ_m is the correlation time due to the tumbling of the whole molecule. The effective internal correlation time describing the rapid internal motions is described by τ_e in the equation:

$$\frac{1}{\tau} = \frac{1}{\tau_m} + \frac{1}{\tau_e} \quad (2)$$

In some cases an additional term, R_{ex} , as shown in eq 3 is needed to model transverse relaxation rates where there were additional contributions to relaxation, other than dipole-dipole interactions and chemical shift anisotropy, such as conformational exchange averaging

$$\frac{1}{T_2} = \frac{1}{T_{2(\text{DD})}} + \frac{1}{T_{2(\text{CSA})}} + R_{\text{ex}} \quad (3)$$

where the subscripts DD and CSA indicate the contributions from dipole-dipole and chemical shift anisotropy to transverse relaxation. Several variations of the function described by eq 3 were used to fit the experimental data: $\tau_e = 0$, τ_e included as a fitting parameter, $\tau_e = 0$ and including the term R_{ex} to account for conformational exchange, and with both τ_e and R_{ex} as fitting parameters.

NOE-Derived Restraints. NOE cross-peaks from the two- and three-dimensional NOESY experiments were classified as strong, medium, or weak corresponding to distance restraints of 1.9–2.7, 1.9–3.3, and 1.9–5.0 Å, respectively. Upper distance restraints involving nonstereospecifically assigned methylene, aromatic, and methyl protons were adjusted for center averaging (Wuthrich et al., 1983).

Torsion Angle Restraints. Torsion angle restraints for the ϕ angles were derived from an analysis of the $^3J_{\text{HN,H}\alpha}$ coupling constants measured from three-dimensional HNHA spectra. Restraints were included in the early rounds of calculations for the following coupling constants: >8.5 Hz ($-140 \pm 30^\circ$), <5.5 Hz ($-60 \pm 30^\circ$). Since some coupling constants can correspond to more than one torsion angle, restraints were only included for regular secondary structural elements as determined from the NOE data. During later stages of structure refinement if only one value of ϕ was consistent with the structure and the coupling constant, a corresponding restraint with large bounds ($\pm 50^\circ$) was included. In some cases the ϕ angle was simply restricted to negative values.

Hydrogen-Bonding Restraints. Slowly exchanging amide hydrogens were identified qualitatively from a series of two-dimensional ^1H - ^{15}N HMQC spectra recorded at various time intervals after a lyophilized uniformly ^{15}N -labeled protein sample was dissolved in D_2O . Complementary information about rapidly exchanging hydrogens was obtained from a series of WEX-filtered HMQC spectra. Hydrogen bond restraints were introduced only after initial rounds of calculations revealed the fold of the protein. Distance restraints of 1.5–2.3 Å for ^1H - O_C and 2.4–3.3 Å for N_H - O_C were added for secondary structural elements where the acceptor-donor pairs were unambiguous.

Structure Calculations. Structure calculations were performed using the computer program X-PLOR version 3.1 (Brünger, 1992). A hybrid distance geometry/simulated annealing protocol as described in the manual was used. The value of the NOE and torsion angle potentials were calculated with force constants of $50 \text{ kcal mol}^{-1} \text{ \AA}^{-2}$ and $200 \text{ kcal mol}^{-1} \text{ rad}^{-2}$, respectively.

Initial calculations started from a linear polypeptide template with random backbone angles. An iterative approach similar to that described by Powers et al. (1993) was employed in later rounds of refinement. Additional experimental restraints were included as the quality of the structures improved and ambiguities in the NOE data were resolved. A simulated annealing refinement was repeated after each update of the NOE list. The final round of calculations was also started from a linear polypeptide template.

The abrupt distance cutoff ranges caused some NOEs that were close to the boundary of two ranges to be systematically violated. In such cases, these NOEs were reclassified into

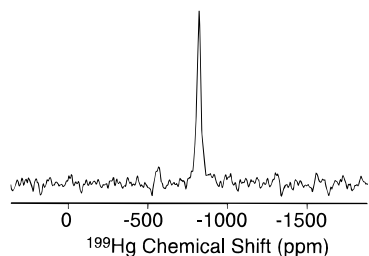


FIGURE 1: ^{199}Hg NMR spectrum of $\text{Hg}(\text{II})$ bound to merP in solution obtained by direct detection at 89.5 MHz.

the next weaker class. As discussed by Clore et al. (1993), this improves accuracy at the expense of precision.

The five non-native residues at the N-terminus of the expressed protein were initially included in the calculations but were later omitted. They were not restrained by the experimental NMR data, and it was clear they did not form an integral part of the structural fold of merP in solution.

In the structure calculations for the mercury-bound form of merP the $\text{Hg}-\text{S}$ dicoordinate bond length of 2.33 Å was specified (Utschig et al., 1993) with a force field of 500 kcal mol $^{-1}$ Å $^{-2}$. The force field for all other bonds was 1000 kcal mol $^{-1}$ Å $^{-2}$. The $\text{S}-\text{Hg}-\text{S}$ bond angle was initially set to 180° with a force field of 70 kcal mol $^{-1}$ rad $^{-2}$, which is significantly lower than the 500 kcal mol $^{-1}$ rad $^{-2}$ used for all other bond angles.

RESULTS

Expressed MerP Protein. MerP prepared from the MBP fusion protein has five additional amino acids at the N-terminus. In order to avoid confusion, we utilize a numbering system that correlates directly with the wild-type amino acid sequence of merP. Residue 1 is Ala, and the extra residues that remain attached to the N-terminus after cleavage are designated -5 through -1. Amino acid analysis confirmed that the protein has the expected amino acid composition. Two-dimensional $^1\text{H}-^{15}\text{N}$ HMQC spectra obtained from samples of uniformly ^{15}N -labeled 77-residue merP isolated from the MBP fusion protein and 72-residue native merP isolated after expression from other vectors without the use of a fusion protein are nearly identical. Three of the five expected extra peaks are present in the spectrum of the fusion-derived protein, and the amide ^1H and ^{15}N chemical shift frequencies of the first few residues are slightly shifted. The extra resonances show no NOEs to residues other than those adjacent in the sequence, which suggests that they are not structured and do not interact with the rest of the protein.

Coordination of Metal. The coordination geometry of metal binding proteins can be probed by ^{199}Hg NMR spectroscopy as demonstrated by O'Halloran and co-workers for several proteins, including the regulatory protein merR of the *mer* operon (Utschig et al., 1995). ^{199}Hg NMR spectroscopy is ideal for studying the coordination geometry of merP since Hg^{2+} is its native metal and ^{199}Hg is a spin $S = 1/2$ nucleus with a chemical shift range of more than 3000 ppm that is highly sensitive to its ligands. Figure 1 contains the directly detected one-dimensional ^{199}Hg NMR spectrum of $\text{Hg}(\text{II})$ bound to merP in aqueous solution. The chemical shift of bound mercury is -816 ppm, which is within the range observed for linear bicoordinate aliphatic thiolate compounds [-816 and -985 ppm for $\text{Hg}(\text{S}-n\text{-Pr})_2$ and $\text{Hg}(\text{SEt})_2$, respectively] (Kubicki et al., 1981). In contrast, the ^{199}Hg chemical shift observed for $\text{Hg}(\text{II})$ bound to merR which is tricoordinate (three Cys residues) is -106 ppm (Utschig et al., 1995), and this result correlates well with those for structurally characterized tricoordinate aliphatic thiolate compounds. Thus, the chemical shift value of mercury bound to merP shown in Figure 1 demonstrates that the metal is bicoordinate and not tricoordinate.

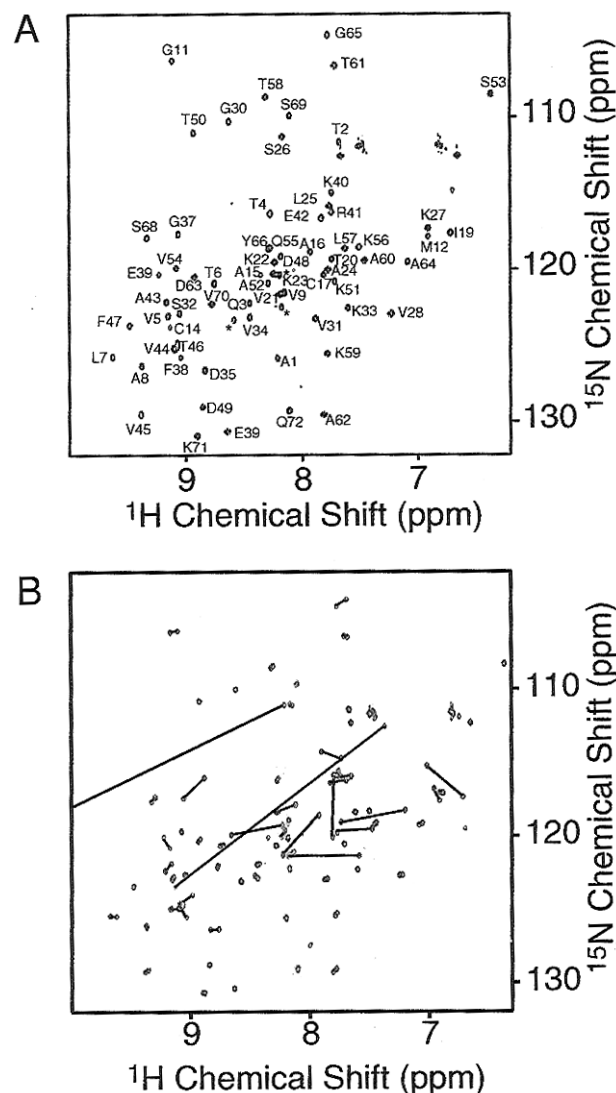


FIGURE 2: (A) Two-dimensional HMQC $^1\text{H}-^{15}\text{N}$ spectrum of uniformly ^{15}N -labeled reduced merP. All resonances have been assigned. The peak belonging to T13 (10.49 ^1H ppm) is often weak and is not shown on this plot. (B) Overlay of two-dimensional HMQC spectra of reduced and mercury-bound forms of merP. Resonances from reduced merP are in red and those from the mercury-bound form of merP are in blue. Lines correlate resonances that shift substantially upon binding $\text{Hg}(\text{II})$.

the ^{199}Hg chemical shift observed for $\text{Hg}(\text{II})$ bound to merR which is tricoordinate (three Cys residues) is -106 ppm (Utschig et al., 1995), and this result correlates well with those for structurally characterized tricoordinate aliphatic thiolate compounds. Thus, the chemical shift value of mercury bound to merP shown in Figure 1 demonstrates that the metal is bicoordinate and not tricoordinate.

Protein NMR Spectra. The two-dimensional $^1\text{H}-^{15}\text{N}$ HMQC spectrum of uniformly ^{15}N -labeled reduced merP in Figure 2A displays essentially complete resolution among all amide resonances. The line widths in both ^1H and ^{15}N frequency dimensions are narrow, and there is excellent chemical shift dispersion in both dimensions as well. Two-dimensional $^1\text{H}-^{15}\text{N}$ HMQC spectra of the mercury-bound and reduced forms of merP are superimposed in Figure 2B. A number of amide resonances shift significantly when the protein binds mercury. Since the resonances from all backbone sites have been identified and assigned for both

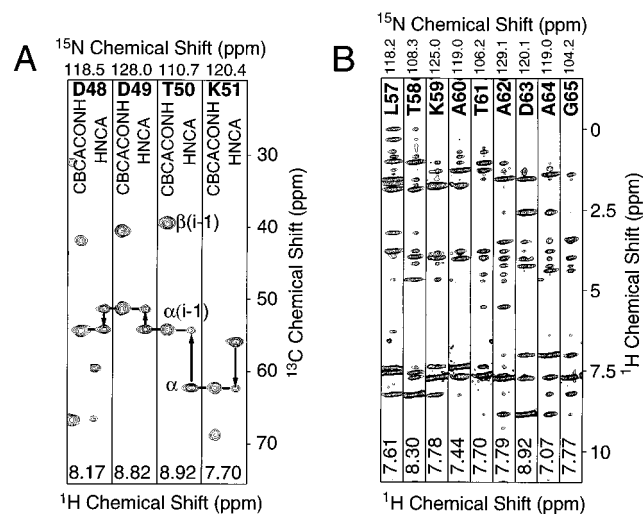


FIGURE 3: (A) $^1\text{H}/^{13}\text{C}$ strips taken from three-dimensional HNCA and CBCACONH spectra of reduced merP at 600 MHz. The strips are interleaved (CBCACONH, left; HNCA, right). The C^α resonance assignment pathway is indicated. (b) $^1\text{H}-^1\text{H}$ strips at different ^{15}N chemical shifts from a three-dimensional ^{15}N resolved NOESY/HMQC spectrum obtained at 750 MHz. The NOE mix time was 100 ms. The residues are from helix H2.

forms of the protein (except for A15 in the mercury-bound form), lines are used to correlate the resonances most strongly affected by metal binding.

A combination of three-dimensional ^{15}N -separated NOESY/HMQC and HOHAHA/HMQC (Marion et al., 1989) and triple-resonance experiments were used to sequentially assign resonances of the protein. HNCA spectra show a strong correlation peak from the amide hydrogen and nitrogen resonances to the interresidue α -carbon resonance and a weak correlation peak to the α -carbon resonance of the previous residue (Bax & Ikura, 1991), which provides the sequential residue connection needed for assignments. However, some residues showed only one carbon peak due to a degenerate ^{13}C chemical shift or the interresidue correlation being too weak to detect, and in these cases the HNCOCA or CBCACONH experiments were essential in order to complete the assignments. The CBCACONH and HNCOCA experiments gave strong correlations to C^α resonances in the previous residue, but the CBCACONH experiment provides the β -carbon chemical shift frequencies as well. Stretches of amide resonances were aligned sequentially by matching the C^α chemical shift frequencies as illustrated in Figure 3A. Ambiguities in the assignments could generally be resolved by referring to the NOE/HMQC data and looking for interresidue correlations, as shown in Figure 3B.

The C^β chemical shifts observed in the CBCACONH experiment were useful in identifying the most probable type of amino acid associated with each C^α and C^β chemical shift (Grzesiek & Bax, 1993a). Gly residues have upfield chemical shifts and give rise to only one interresidue peak. Thr, Ser, and Ala residues also have distinctive $\text{C}^\alpha/\text{C}^\beta$ chemical shift pairs; for example, in Figure 3A the C^β chemical shift of T50 is downfield of the C^α which is typical of Thr residues. All amino acid type assignments were compared to those predicted from the ^{15}N resolved TOCSY/HMQC spectrum. In this way connected stretches of residues could be placed uniquely in the protein sequence. Breaks in the sequential connectivity occurred at prolines.

For the mercury-bound merP ^{15}N resolved three-dimensional TOCSY/HMQC and NOESY/HMQC spectra were sufficient to make the sequential assignments, since only a subset of resonances had to be reassigned from those observed in the reduced form of merP.

Aromatic side chain ^1H resonance assignments were determined from two-dimensional NOESY (50 and 125 ms mix times) and TOCSY (80 ms) experiments in D_2O solution. Connectivities were established in the standard way (Wüthrich, 1986) and then cross-checked with resonances observed in the ^{15}N resolved three-dimensional experiments.

The experiments in D_2O solution were useful for obtaining critical side chain to side chain NOEs for helix-helix and sheet-helix contacts. Several resonances, in particular, V21 (γ -methyls), L57 (δ -methyls), and L25 (δ -methyls), are upfield shifted and well separated; these, and those from the aromatic residues F47 and Y66, provided many unambiguous NOEs essential for determining the overall protein fold. The upfield-shifted resonances also provided a convenient monitor of the binding of mercury to merP since they are single isolated peaks in the one-dimensional ^1H NMR spectrum; for example, the methyl resonance from V21 shifts downfield when mercury binds to the protein.

Summaries of the short- and medium-range NOEs and other measurements for the reduced and mercury-bound forms of merP are shown in Figure 4. There are clearly two helices in merP, as indicated by the presence of $\alpha\text{N}(i+3)$ and $\alpha\text{N}(i+4)$ and strong $\text{NN}(i+1)$ NOEs. There are four regions of β sheet, as indicated by strong $\alpha\text{N}(i+1)$ and only weak $\text{NN}(i+1)$. The chemical shift index data (Wishart et al., 1991, 1992) in Figure 4 agrees well with the secondary structure predictions from the NOE data with helical H^α chemical shifts below and β sheet H^α chemical shifts above those of a random coil polypeptide. The secondary structure elements at the top of Figure 4 are referred to as B1, H1, B2, B3, H2, and B4.

Structure Calculations. A total of 972 distance restraints were derived for the NMR experiments on the mercury-bound form of merP. Of these, 221 were interresidue, 323 sequential, and 428 medium and long range ($|i-j| \geq 2$). In addition, 67 torsion angle and 56 hydrogen bond restraints were used in the structure calculations. The total of 1095 corresponds to 15.2 restraints per residue. For the reduced form of merP 918 NOE distance restraints were used, consisting of 210 interresidue, 298 sequential, and 418 medium and long range as well as 61 dihedral and 56 hydrogen bond restraints. This is a total of 1035 restraints (14.4 per residue).

From the 80 structures that resulted from the final round of calculations for both mercury-bound and reduced forms of merP, 29 (mercury-bound) and 36 (reduced) contained no upper bound NOE violations greater than 0.5 \AA or dihedral angle violations greater than 5° . The 20 lowest energy for each form were used for further analysis. Pertinent structural statistics are shown in Table 1. In general, all structures have good covalent geometry as shown by small deviations from idealized geometry. Ramachandran plots of ϕ, ψ angles are shown in Figure 5A,C for residues 3-71. The majority of residues are in energetically favorable regions. A few residues in loop regions have significantly positive values but still fall in energetically favorable regions of the Ramachandran plot.

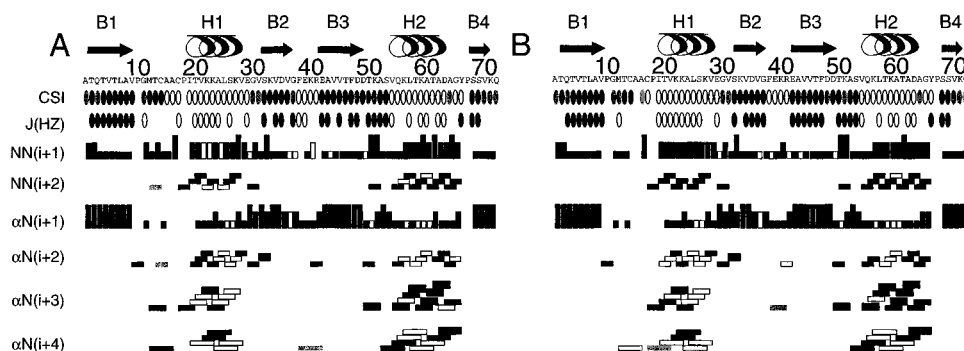


FIGURE 4: Short-range interaction summaries for reduced and mercury-bound forms of merP. Secondary structural elements are indicated at the top of the figure. (A) Reduced merP. (B) Mercury-bound merP. Black boxes indicate the presence of an NOE and protons that are less than 5 Å apart; unfilled boxes represent NOEs that are obscured or partially overlapped and were not used in structural calculations; shaded boxes are for NOEs that are not present in the alternative form of the protein. CSI: chemical shift index for H_{α} protons; filled ovals = 1 (sheet); shaded ovals = 0 (coil); unfilled ovals = -1 (helical). $J(\text{Hz})$: $^3J_{\text{HN-H}\alpha}$ coupling; filled ovals ≥ 8.5 Hz; unfilled ovals = ≤ 5.5 Hz.

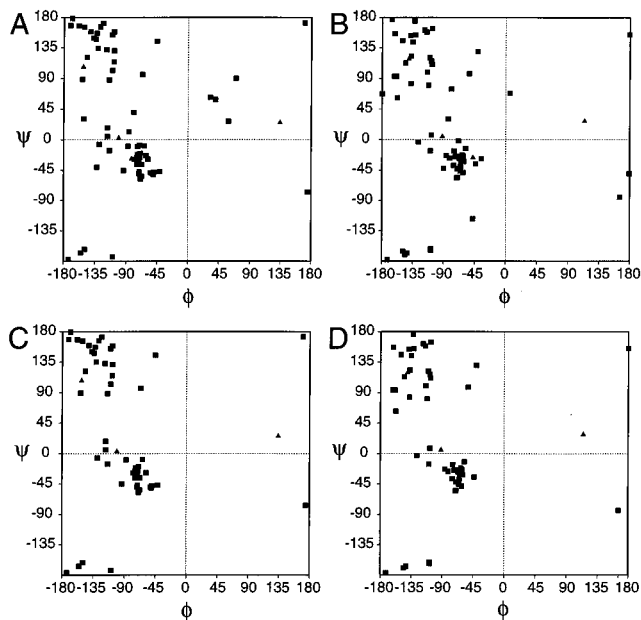


FIGURE 5: Ramachandran ϕ, ψ plots of merP for the lowest energy structure from each ensemble: (A) reduced form, residues 3–71; (B) mercury-bound form, residues 3–71; (C) reduced form, residues 3–9, 19–37, and 42–71; (D) mercury-bound form, residues 3–9, 19–37, and 42–71. Glycines are indicated by small triangles.

Superpositions of the 20 lowest energy structures of both forms of merP are shown in Figure 6A,B. Nearly all of the polypeptide has a well-defined structure in both mercury-bound and reduced forms of merP, as indicated in the rmsd values listed in Table 2. The rmsd to the average for residues 3–71 is 0.361 and 0.355 Å for the reduced and mercury-bound forms of merP, respectively. If residues 10–18, which constitute the metal binding loop, are excluded, these values drop to 0.339 and 0.299 Å. If only those residues whose amide and nitrogen chemical shifts do not change significantly are included in the rmsd calculations (as indicated in Figures 5 and 6), these values drop even further to 0.322 and 0.270 Å. The spectra of the reduced form of the protein tend to have more chemical shift overlap, which limits the number of restraints that could be confidently extracted from the data. If residues 11–18 and 38–41, which form a turn near the metal binding site, are excluded from the Ramachandran plot as shown in Figure 5B,D, the differences between the two forms are minimal.

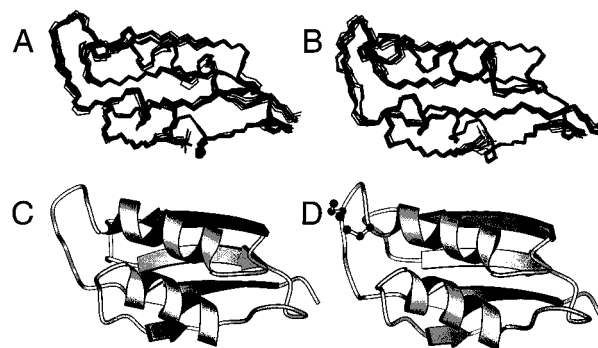


FIGURE 6: (A) Reduced merP. (B) Mercury-bound merP. Superposition of the 20 lowest energy calculated structures. Structures were least squares fit using the heavy backbone atoms C, C^{α} , and N atoms of residues 3–71. Residues 1–72 are shown for all representations of the structure of merP. (C) Reduced merP. (D) Mercury-bound merP. Schematic representations of merP. Diagrams were generated with the program MOLSCRIPT (Kraulis, 1991).

Dynamics. Comparisons of T_1 , T_2 , heteronuclear NOE, and the fitted order parameter S^2 for reduced and mercury-bound forms of merP are shown in Figure 7. The missing bar graph positions correspond to proline residues without amide resonances or other amino acids whose amide resonances partially overlap, making relaxation measurements unreliable. Residues 1, 2, and 72 are significantly mobile on a fast time scale as indicated by the low values of the order parameter S^2 , the lower values of the heteronuclear NOEs, and the higher values of T_1 and T_2 . In addition, the residues in the loop connecting strand B3 and the second helix (residues 51–53) show some evidence of mobility. This is most obvious in the values of T_1 (Figure 7E,F), which are significantly longer than for the majority of residues in the protein. The largest differences, however, between the two forms of the proteins are in the values of T_2 observed for residues 11–18 in the metal binding loop. The T_2 values for these residues in the reduced form of the protein are shorter than those observed in the mercury-bound form. In contrast, there are no apparent differences in the values of T_1 or NOE observed for these residues. This resulted in the need for an exchange term, R_{ex} , in the fitting of the order parameter for residues 11–18. The value of the exchange parameter is included in Figure 7A,B where it provided the best fit of all considered models described in the Materials and Methods section.

Table 2: Structural Statistics and Atomic rms Differences^a

type	(A) Structural Statistics			
	reduced		mercury	
rms deviations from exptl distance restraints (Å)	0.039 ± 0.0013		0.034 ± 0.0013	
rms deviations from exptl dihedral restraints (deg)	0.82 ± 0.16		0.88 ± 0.11	
rms deviations from ideal covalent geometry				
bonds (Å)	0.0039 ± 0.00016		0.0037 ± 0.00010	
angles (deg)	0.70 ± 0.015		0.73 ± 0.017	
impropers (deg)	0.58 ± 0.021		0.59 ± 0.027	

type	(B) Atomic rms Differences (Å)			
	reduced		mercury	
	backbone ^b	all non-H	backbone ^b	all non-H
$\langle SA \rangle$ vs $\langle \overline{SA} \rangle$ ^c	0.361 ± 0.0628	0.838 ± 0.0850	0.355 ± 0.0586	0.911 ± 0.0687
$\langle SA \rangle$ vs $\langle \overline{SA} \rangle$ selected ^d	0.339 ± 0.0625	0.844 ± 0.0957	0.299 ± 0.0444	0.872 ± 0.0661
$\langle SA \rangle$ vs $\langle SA \rangle$ similar ^e	0.322 ± 0.0735	0.753 ± 0.1000	0.270 ± 0.0408	0.780 ± 0.0797

^a $\langle SA \rangle$ represents the 20 lowest energy structures and $\langle \overline{SA} \rangle$ represents the mean atomic structure obtained by averaging the ensemble after a least-squares fit of heavy backbone atoms (N, C $^{\alpha}$, and C $^{\prime}$) for residues 3–71. ^b For heavy atoms N, C $^{\alpha}$, and C $^{\prime}$. ^c For residues 3–71. ^d For residues 3–9 and 19–71, which excludes the binding loop. ^e For all residues whose chemical shifts are similar for both reduced and mercury-bound forms, 3–9, 19–36, and 43–71.

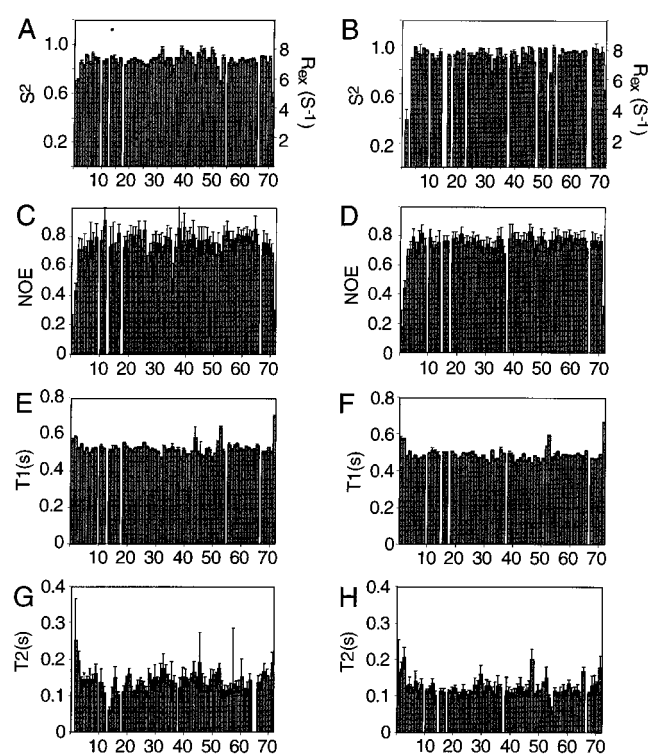


FIGURE 7: Experimental relaxation parameters and calculated parameters for each residue in reduced merP and mercury-bound merP. (A) Reduced merP and (B) mercury-bound merP calculated order parameters S_2 . The values in black boxes on the secondary axis represent the exchange term R_{ex} needed to fit the data to order parameters for some residues. (C) Reduced merP and (D) mercury-bound merP heteronuclear 1H – ^{15}N NOEs. (E) Reduced merP and (F) mercury-bound merP and T_1 values. (G) Reduced merP and mercury-bound merP T_2 values.

Description of the Structure. MOLSCRIPT (Kraulis, 1991) representations of the structures of the reduced and mercury-bound forms of merP are shown in panels C and D of Figure 6, respectively. The two α helices are formed by residues 19–27 for mercury-bound merP (17–27 in reduced form) and residues 54–64 in both forms. The two helices lie above the plane of a four-strand β sheet formed by residues 3–9, 31–37, 42–47, and 69–70. The four-strand β sheet has a slight left-handed twist common in many antiparallel β sheets. This twist is more pronounced in the

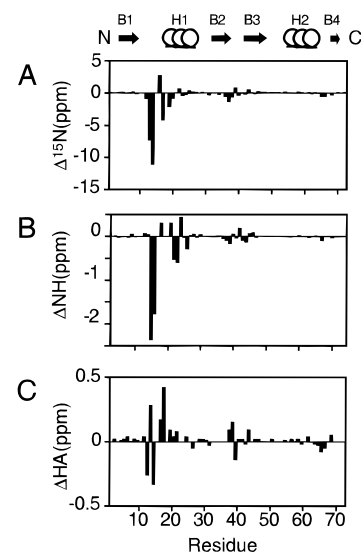


FIGURE 8: Chemical shift changes upon addition of mercury to reduced merP. The values represent $[\delta(\text{mercury}) - \delta(\text{reduced})]$. The secondary structural elements are indicated above. (A) Nitrogen chemical shift change. (B) H^N proton chemical shift change. (C) H^{α} proton chemical shift change.

last short strand. A β bulge between residues S32, K33, and T46 breaks the sheet at the beginning of strand B2. The helices are roughly parallel and are oriented at an angle of about 15° relative to the axis of the β sheet. The interhelical angle is about 50° . This follows the twist of the β sheet as the helices are packed against the sheet. The long loop connecting strand B1 and the first helix contains the metal binding site with the GMTCAAC sequence. In the mercury-bound form the two Cys residues lie above the loop toward the surface of the protein. The S–Hg–S bond angle 177° is close to linear.

Chemical Shift Differences. Figure 2B contains the two-dimensional 1H – ^{15}N HSQC spectra of reduced and mercury-bound forms of merP. There are dramatic differences in the chemical shifts of a few amide resonances. The chemical shift differences for the amide 1H and ^{15}N and $^1H^{\alpha}$ resonances are plotted in Figure 8. Significant resonance shifts are localized to three main regions of the protein. The largest changes occur in the loop connecting β sheet strand B1 and helix H1 and part of the way into helix H1. This is the region

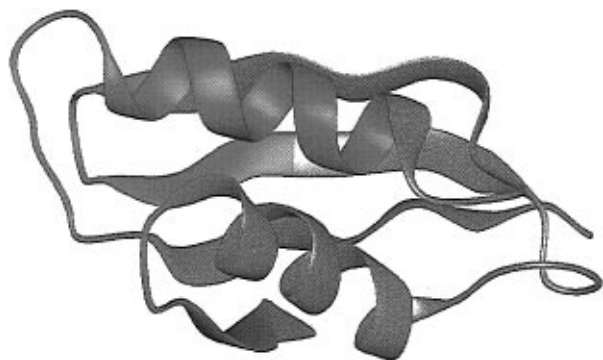


FIGURE 9: Ribbon representation of reduced merP. Blue indicates those residues whose chemical shifts did not change significantly upon addition of mercury. Red indicates regions of significant change.

that contains the GMTCAAC binding site of the mercury. Smaller changes occur in the region between strands B2 and B3. This turns out to be directly below the proposed binding loop in the three-dimensional fold. The final region of shift change is smaller, but still significant. This is the turn connecting helix H2 and strand B4. Again, this is in the vicinity of the binding loop in the three-dimensional structure. Figure 9 contains a representation of merP colored to show the regions with the largest chemical shift differences between the two forms of merP.

DISCUSSION

Structure of MerP. Both the reduced and mercury-bound forms of merP have essentially the same global fold, which consists of two antiparallel helices overlaying a four-strand β sheet. The secondary structure and overall fold derived from earlier homonuclear NMR experiments on the oxidized form of merP (Eriksson & Sahlman, 1993) are consistent with the three-dimensional structures of the reduced and mercury-bound forms of merP shown in Figure 6. The SCOP database (Murzin et al., 1995) indicates that the $\beta\alpha\beta\beta\alpha\beta$ fold defines a class of $\alpha\beta$ proteins with antiparallel β sheets and segregated α and β sections. The fold can be described as an α - β sandwich characteristic of "ferredoxin-like" proteins which have diverse functions. This class of proteins includes small proteins and domains of larger proteins such as RNA binding protein domains, DNA binding protein domains, acyl phosphatases, and the phosphoglycerate dehydrogenase regulatory domain. They do not appear to have a functional theme in common with other heavy metal binding proteins, and the active sites to these proteins vary dramatically. For example, one of the largest groups of protein that gave this fold is the family of RNA binding proteins. Even among members of this family of proteins there is considerable functional diversity. The binding site of these proteins is usually localized to the outer surface of the β sheet (Bird & Dreyfuss, 1994). This is very different from the situation found for merP.

The spectroscopic differences between the two forms of the protein, as highlighted in Figure 9, are localized near the GMTCAAC-containing loop connecting the first strand of the sheet to the first helix. They involve residues distant in the primary sequence but close in the folded structure including those near the turns including residues 38–41 and 64–66. The finding of changes in the fluorescence of Y66 upon binding Hg(II) is consistent with this (Summers,

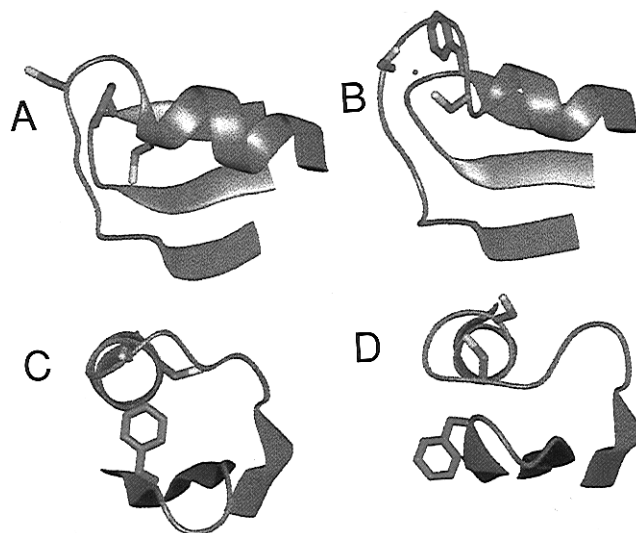


FIGURE 10: Ribbon representations of the segment of merP containing the metal binding loop, part of helix H1, and the loop connecting β strands B2 and B3. The cysteine residues, C14 and C17, and the aromatic ring, F38, are highlighted in red. (A) Reduced merP, view from above. (B) Mercury-bound merP, view from above. (C) Reduced merP, end view looking down helix H1. (D) Mercury-bound merP, end view looking down helix H1.

personal communication). The structural representations in Figure 10 allow detailed comparisons of the metal binding loop in the two forms of the protein. The two Cys residues are much further away from each other in the reduced form than in the mercury-bound form. Binding of mercury causes a slight unwinding of the helix as the two cysteines become closer. Another difference is the position of the aromatic residue F38 which lies below the metal binding loop. In the reduced form the side chain is oriented toward the binding loop. The two-dimensional homonuclear NOE spectrum of the reduced form of merP has more than eight NOE cross-peaks between Phe ring resonances and those from residues 9 through 17. In contrast, the aromatic ring moves closer to the surface of the protein in the mercury-bound form, and no NOE cross-peaks are observable from the same Phe ring hydrogens. The movement of this aromatic ring may account for the dramatic ^{15}N and ^1H chemical shift differences for some of the backbone resonances in the two forms of the protein.

The S–Hg–S bond is approximately linear in the structure of the mercury-bound form of merP, and this is confirmed by the ^{199}Hg chemical shift of the bound mercury ion. The coordination geometries of many model compounds have been examined (Utschig et al., 1993; Wright et al., 1990). The most common primary coordination number for Hg(II) is 2. These compounds have covalent bond lengths that vary between 2.316 and 2.361 Å and bond angles that vary between 180.0° and 167.4° (Wright et al., 1990). Distortions from linearity are generally caused by longer secondary bonding interactions found in the solid state. MerP clearly binds Hg(II) with two Cys ligands. This is in agreement with mutagenesis that show both Cys residues to be essential for specific mercury binding to the protein (Sahlman & Skärfstad, 1993). The slight deviation of the S–Hg–S bond linearity may be caused by an interaction with a water molecule. The binding site of merP is very different from that of merR, which has a tricoordinate binding site (Utschig et al., 1993).

Another difference between the two forms of merP is their dynamics. An increase in T_1 or T_2 for some resonances compared to those from the bulk of the protein generally suggests that the residues undergo some extra modes of rapid motion. However, when there is a drop in T_2 , with no related drop in T_1 , this does not suggest there is less motion but rather that the motion is on a different time scale. The greater number of exchange terms needed to fit the order parameter S^2 for the reduced form of the protein suggests that the binding loop may undergo an additional motion on a slow time scale. There does not appear to be any evidence of multiple conformations in the NOE data, as there are fewer NOEs per residue compared to the bulk of the protein through this binding loop for both forms of the protein. This is partly due to the exposed and extended nature of this loop. Although the loop as a whole has a single conformation, it may "flap" or "breathe" slowly without a bound metal. When the Cys residues interact with the mercury, they stabilize the entire loop, giving it a very well-defined conformation.

The primary role of merP appears to be that of a scavenger of free Hg(II) in the cell periplasm (Silver & Walderhaug, 1995). After binding Hg(II), merP passes it to the next protein in the chain, merT, which transports it across the cell membrane into the cytoplasm where it is reduced by the enzyme mercuric reductase to Hg(0). In this context, it is not surprising that major structural changes are not observed when merP binds mercury. A global structural rearrangement could be counterproductive, since it might move the mercury ion away from the surface of merP to a place where it would be inaccessible to merT. Nonetheless, the metal binding loop does appear to have some conformational flexibility, and a transient intermediate conformation may be involved in passing Hg(II) to merT from merP. The "bucket brigade" mechanism, suggested as a way of passing the mercury from protein to protein in the detoxification pathway (Brown et al., 1991), would be consistent with the structures of the reduced and mercury-bound forms of merP. As yet, however, no suggestions have been made about the molecular mechanisms of how the proteins of the bacterial mercury detoxification system interact. The hydrophobic "patch" created by the movement of Phe38 toward the surface of the protein might possibly be important for either protein-protein interaction with merT or for some interaction with the lipid bilayer in which merT is located. Phe38 is highly conserved among the merP sequences from a wide variety of bacteria. In the merP-like domains of mercuric reductase (merA), this residue is either a Tyr or Phe. Interestingly, in the heavy metal associated regions from the copper transport proteins associated with Menkes and Wilson diseases, the corresponding residue is another highly conserved hydrophobic residue, leucine. This difference may be partially related to the metal specificities of the different transport systems. Structure determination of merP-like domains from other proteins and organisms, including those that bind to other metals, should provide further information about the factors that contribute to the strength and specificity of metal binding. Indeed, the structure of merP itself contributes to the description of merA, since that protein contains two merP-like domains near its N-terminus but they could not be visualized in its crystal structure due to disorder (Schiering et al., 1991). The structure determination of merT, which is believed to accept the mercury ion from merP for transport across the membrane, is in progress. The combina-

tion of the structures of merA, merP, and merT should provide considerable insight into the structural biology of heavy metal bioremediation.

ACKNOWLEDGMENT

We thank Nancy Hamlett for many helpful discussions in the initial stages of this investigation as well as Matt Harris and Dave Karlton for preparing the original pHK1 plasmid while working in her laboratory at Swarthmore College. We also thank Anne Summers for helpful discussions and for providing results prior to publication and Neil Farrow for computer programs and advice on their use.

SUPPORTING INFORMATION AVAILABLE

Two tables giving chemical shift assignments for the mercury-bound merP and the reduced merP (8 pages). Ordering information is given on any current masthead page.

REFERENCES

- Ansari, A. Z., Chael, M. L., & O'Halloran, T. V. (1992) *Nature* 355, 87–89.
- Bax, A., & Ikura, M. (1991) *J. Biomol. NMR* 1, 99–104.
- Bax, A., Griffey, R. H., & Hawkins, B. L. (1983) *J. Magn. Reson.* 55, 301.
- Bird, C. G., & Dreyfuss, G. (1994) *Science* 265, 615–621.
- Brown, N. L. (1985) *Trends Biochem. Sci.*, 400–403.
- Brown, N. L., Camakaris, J., Lee, B. T. O., Williams, T., Morby, A. P., Parkhill, J., & Rouch, D. A. (1991) *J. Cell Biol.* 46, 106–114.
- Brünger, A. T. (1992) *X-PLOR Version 3.1. A System for X-ray Crystallography and NMR*, Yale University Press, New Haven, CT.
- Chelly, J., Tümer, Z., Tønnesen, T., Petterson, A., Ishikawa-Brush, Y., Tommerup, N., Horn, N., & Monaco, A. P. (1993) *Nat. Genet.* 3, 14–19.
- Clore, G. M., Robien, M. A., & Gronenborn, A. M. (1993) *J. Mol. Biol.* 231, 82–102.
- Eriksson, P. O., & Sahlman, L. (1993) *J. Biomol. NMR* 3, 613–626.
- Farrow, N. A., Muhandiram, R., Singer, A. U., Pascal, S. M., Kay, C. M., Gisk, G., Shoelson, S. E., Pawson, T., Forman-Kay, J. D., & Kay, L. E. (1994) *Biochemistry* 33, 5984–6003.
- Foster, T. J. (1987) *CRC Crit. Rev. Microbiol.* 15, 117–140.
- Grzesiek, S., & Bax, A. (1992) *J. Am. Chem. Soc.* 114, 6291–6293.
- Grzesiek, S., & Bax, A. (1993a) *J. Biomol. NMR* 3, 185–204.
- Grzesiek, S., & Bax, A. (1993b) *J. Am. Chem. Soc.* 115, 12593–12594.
- Hahn, L. J., Kloiber, R., Leininger, R. W., Vimy, M. J., & Lorscheider, F. L. (1990) *FASEB J.* 4, 3256–3260.
- Helmann, J. D., Schewchuk, L. M., & Walsh, C. T. (1990) *Adv. Inorg. Biochem.* 8, 33–61.
- Kay, L. E., Torchia, D. A., & Bax, A. (1989) *Biochemistry* 28, 8972–8979.
- Kay, L. E., Ikura, M., Tschudin, R., & Bax, A. (1990) *J. Magn. Reson.* 89, 496–514.
- Kay, L. E., Nicholson, L. K., Delaglio, F., Bax, A., & Torchia, D. A. (1992) *J. Magn. Reson.* 97, 359–375.
- Kraulis, P. J. (1991) *J. Appl. Crystallogr.* 24, 946–950.
- Kubicki, M. M., Kergoat, R., Guerchais, J. E., Bkouche-Waksman, I., Bois, C., & L'Hairdon, P. (1981) *J. Organomet. Chem.* 219, 329–343.
- Levitt, M. H. (1982) *J. Magn. Reson.* 47, 328–330.
- Lipari, G., & Szabo, A. (1982a) *J. Am. Chem. Soc.* 104, 4546–4559.
- Lipari, G., & Szabo, A. (1982b) *J. Am. Chem. Soc.* 104, 4559–4570.
- Lorscheider, F. L., Vimy, M. J., & Summers, A. O. (1995) *FASEB J.* 9, 504–508.
- Lund, P. A., & Brown, N. L. (1987) *Gene* 52, 207–214.

- Lutsenko, S., & Kaplan, J. H. (1995) *Biochemistry* 34, 15607–15613.
- Marion, D., Driscoll, P. C., Kay, L. E., Wingfield, P. T., Bax, A., Gronenborn, A., & Clore, G. M. (1989) *Biochemistry* 28, 6150–6156.
- Mercer, J. F. B., Livingston, J., Hall, B., Paynter, J. A., Begy, C., Chandrasekharappa, S., Lockhart, P., Grimes, A., Bhave, M., Siemieniak, D., & Glover, T. W. (1993) *Nat. Genet.* 3, 20–25.
- Misra, T. K., Brown, N. L., Fritzinger, D. C., Pridmore, R. D., Barnes, W. M., Haberstroh, L., & Silver, S. (1984) *Proc. Natl. Acad. Sci. U.S.A.* 81, 5975–5979.
- Mori, S., O'Neil Johnson, M., Berg, J. M., & van Zijl, P. C. M. (1994) *J. Am. Chem. Soc.* 116, 11982–11984.
- Mori, S., Abeygunawardana, C., O'Neil Johnson, M., & van Zijl, P. C. M. (1995) *J. Magn. Reson. B* 108, 94–98.
- Murzin, A. G., Brenner, S. E., Hubbard, T., & Chothia, C. (1995) *J. Mol. Biol.* 247, 536–540.
- O'Halloran, T. V. (1993) *Science* 261, 715–725.
- Opella, S. J. (1994) in *Membrane Protein Structure: Experimental Approaches* (White, S. H., Ed.) pp 249–267, Oxford University Press, Oxford.
- Piotto, M., Saudek, V., & Sklenar, V. (1992) *J. Biomol. NMR* 2, 661–665.
- Powers, R., Garrett, D. S., March, C. J., Frieden, E. A., Gronenborn, A. M., & Clore, G. M. (1993) *Biochemistry* 32, 6744–6762.
- Rugh, C. L., Wilde, H. D., Stack, N. M., Thompson, D. M., Summers, A. O., & Meagher, R. B. (1996) *Proc. Natl. Acad. Sci. U.S.A.* 93, 3182–3187.
- Sahlman, L., & Skärfstad, E. G. (1993) *Biochem. Biophys. Res. Commun.* 196, 583–588.
- Sanger, F., Niklen, S., & Coulson, A. R. (1977) *Proc. Natl. Acad. Sci. U.S.A.* 74, 5463–5467.
- Schiering, N., Kabsch, W., Moore, M. J., Distefano, M. D., Walsh, C. T., & Pai, E. F. (1991) *Nature* 352, 168–172.
- Shaka, A. J., Barker, P. B., & Freeman, R. (1985) *J. Magn. Reson.* 64, 547–552.
- Silver, S. (1992) *Plasmid* 27, 1–3.
- Silver, S., & Walderhaug, M. (1995) *Bacterial Plasmid-Mediated Resistances to Mercury, Cadmium and Copper*, Springer-Verlag, Berlin.
- Summers, A. O. (1986) *Annu. Rev. Microbiol.* 40, 607–34.
- Utschig, L. M., Wright, J. G., & O'Halloran, T. (1993) *Methods Enzymol.* 226, 71–97.
- Utschig, L. M., Bryson, J. W., & O'Halloran, T. V. (1995) *Science* 268, 380–385.
- von Schägger, H., & Jagow, G. V. (1987) *Anal. Biochem.* 166, 368–379.
- Vuister, G. W., & Bax, A. (1993) *J. Am. Chem. Soc.* 115, 7772–7777.
- Walsh, C. T., Distefano, M. D., Moore, M. J., Shewchuk, L. M., & Verdine, G. (1988) *FASEB J.* 2, 124–130.
- Wishart, D. S., Sykes, B. D., & Richards, F. M. (1991) *J. Mol. Biol.* 222, 311–333.
- Wishart, D. S., Sykes, B. D., & Richards, F. M. (1992) *Biochemistry* 31, 1647–1651.
- Wright, J. G., Natan, M. J., MacDonnell, F. M., Ralston, D. M., & O'Halloran, T. V. (1990) *Mercury(II)-Thiolate Chemistry and the Mechanism of the Heavy Metal Biosensor MerR*, Vol. 38, John Wiley and Sons, New York.
- Wüthrich, K. (1986) *NMR of Proteins and Nucleic Acids*, John Wiley and Sons, New York.
- Wuthrich, K., Billeter, M., & Braun, W. (1983) *J. Mol. Biol.* 169, 949–961.

BI9631632